PERGAMON

International Journal of Heat and Mass Transfer 46 (2003) 631–641

International Journal of HEAT and MASS TRANSFER

www.elsevier.com/locate/ijhmt

Analysis of flow and heat transfer inside oscillatory squeezed thin films subject to a varying clearance

A.-R.A. Khaled [a], K. Vafai [b,*]

[a] Department of Mechanical Engineering, The Ohio State University, Columbus, OH 43210, USA

[b] Department of Mechanical Engineering, University of California, Riverside A363 Bourns Hall, Riverside, CA 92521-0425, USA

Received 31 May 2002; received in revised form 3 August 2002

Abstract

The flow and heat transfer inside a non-isothermal and incompressible thin film having its upper plate slightly inclined from the horizontal and undergoing an oscillatory squeezing motion is investigated in this work. Two models are analyzed: low and large Reynolds number flow models. The corresponding governing equations for each model are properly non-dimensionalized and solved numerically. The main controlling parameters for the dynamic and thermal behavior of the inclined thin film are found to be the amplitude of the upper plate motion, squeezing Reynolds number, squeezing number, thermal squeezing parameter and the dimensionless slope of the upper plate. It is found that fluctuations in the axial and normal velocities are greater for convergent thin films than for divergent thin films. Furthermore, Nusselt numbers and their amplitudes are found to decrease with an increase in the dimensionless slope of the upper plate. Finally correlations are obtained for Nusselt numbers and their corresponding amplitudes for two different thermal conditions: constant wall temperature and uniform wall heat flux.

Keywords: Oscillatory squeezing; Heat transfer; Inertia; Hydrodynamic; Non-flat thin films

1. Introduction

Flow and heat transfer inside thin films have received a significant amount of attention in the recent years because they are widely utilized in many engineering applications such as in lubrication, heat pipes, microchannels and fluidic cells. External disturbances such as unbalances in rotating machines and increased noise levels from the surroundings can result in oscillatory relative motions between the plates surrounding the thin film. Even small oscillating motions can have a substantial impact because the thickness of thin films is very small. Accordingly, the dynamics and thermal characterization of thin films will be altered.

The chambers for chemical and biological detection systems such as fluidic cells for chemical or biological microcantilever probes (Lavrik et al. [1]) are an important example for applications of thin films. Small noise levels that may be present at the boundaries can produce flow instabilities inside the fluidic cells. These disturbances have large influence on the measurements of the detecting elements specially those utilizing microcantilevers. These detecting elements are very sensitive to flow conditions. Therefore, a special design for these fluidic cells such as considering converging or diverging thin films is needed in order to transport the target proteins to the probes with minimum effects of turbulence or thermal disturbances.

There are many studies that have investigated flow in hydrodynamic or squeezed thin films like Langlois [2] who solved analytically the momentum equations for hydrodynamic pressure in isothermal squeezed films with fluid density varying according to the pressure. Later on, towards the end of the 20th century, the interest in

* Corresponding author. Tel.: +1-909-787-2135; fax: +1-909-787-2899.

E-mail address: vafai@engr.ucr.edu (K. Vafai).

0017-9310/03/$ - see front matter
PII: S0017-9310(02)00328-9

Nomenclature

B	thin film length
c_p	specific heat of the fluid
H, h	dimensionless and dimensional thin film thickness
h_c	convective heat transfer coefficient
h_0	reference thin film thickness
k	thermal conductivity of the fluid
Nu	local Nusselt number
Pr	Prandtl number
P_S	thermal squeezing parameter
p	fluid pressure
q	heat flux at the lower plate
R_L, R_S	lateral and squeezing Reynolds numbers
T	temperature in fluid
T_1	fluid inlet temperature
T_2	temperature at the lower and upper plates (CWT)
t	time
U, u	dimensionless and dimensional axial velocities
V, v	dimensionless and dimensional normal velocities
X, x	dimensionless and dimensional horizontal coordinates
Y, y	dimensionless and dimensional vertical coordinates

Greek symbols

Ω, Ω^*	vorticity and dimensionless vorticity
Ψ, Ψ^*	stream function and dimensionless stream function
β	dimensionless squeezing motion amplitude
ε	perturbation parameter
γ	dimensionless frequency
η	variable transformation for Y-coordinate
κ	dimensionless slope of the upper plate
μ	dynamic viscosity of the fluid
θ	dimensionless temperature in flow field
ρ	density of the fluid
σ	squeezing number
τ, τ^*	dimensionless time
υ	kinematic viscosity
ω	reciprocal of a reference time (reference squeezing frequency)
ξ	variable transformation for the dimensionless x-coordinate

Subscripts

L	lower plate
m	average value for velocity and mean bulk value for temperature
U	upper plate
W	lower plate for temperature (UHF)

studying flow inside squeezed thin films increased. Hamza [3] and Bhattacharyya et al. [4] have studied the squeeze effects on the temperature distribution inside the thin film. However their works were concerned with flow between two parallel disks and were simplified to a one-dimensional flow case. Recently, Khaled and Vafai [5,6] considered heat transfer in incompressible squeezed thin films with sinusoidal squeezing for two different models: low and large Reynolds number models. To the authors knowledge the literature lacks studies that are concerned with the effects of pressure squeezing on flow and heat transfer inside convergent or divergent thin films which is related to a number of application such as fluidic cells utilizing detection of biological agents.

In this work, the effects of external squeezing on flow and heat transfer inside thin films having its upper plate slightly inclined are studied. Thin films with positive inclination forms divergent thin films while they become convergent films when the inclination is negative. The governing equations for both low and large Reynolds number flow models are non-dimensionalized and then solved numerically and the influence of squeezing Reynolds number, dimensionless amplitude of the upper plate's motion, squeezing number, thermal squeezing parameter and dimensionless slope for the upper plate are determined on both flow and heat transfer characteristics inside non-flat thin films. Finally, few correlations are generated for Nusselt numbers at the exit of the thin film as functions of both the dimensionless slope of the upper plate and the dimensionless amplitude of the upper plate's motion for two thermal conditions: constant wall temperature (CWT) and uniform wall heat flux (UHF).

2. Problem formulation

Consider a two-dimensional thin film that has a small thickness h compared to its length B. The x-axis is taken in the direction of the length of the thin film, the horizontal direction, while y-axis is taken in the vertical direction along the thickness of the thin film as shown in Fig. 1. The lower plate of the thin film is horizontal and fixed while the upper plate is inclined and allowed to have sinusoidal vertical motion such that the thickness of the thin film can be expressed according to the following relation:

$$h = h_0\left(1 - \beta\cos(\gamma\omega t) + \kappa\frac{x}{B}\right) \tag{1}$$

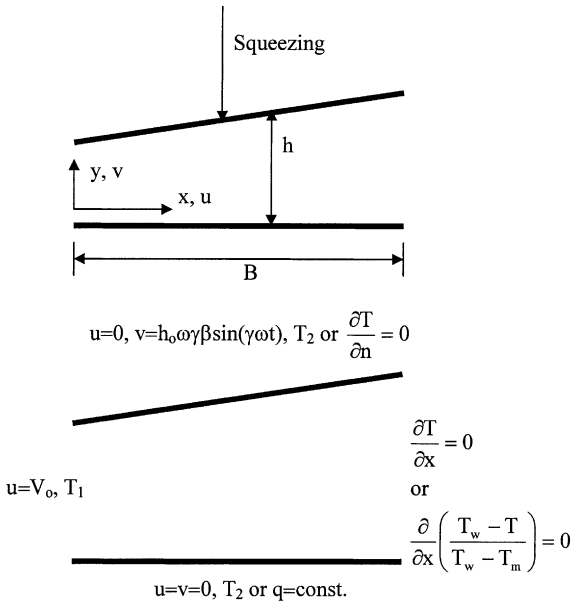

Fig. 1. Schematic diagram and boundary conditions.

where γ is the dimensionless frequency and κ, β and ω are the dimensionless slope of the upper plate of the thin film, dimensionless amplitude of the upper plate's motion and a reference frequency, respectively. It is assumed that the fluid is Newtonian and having constant properties.

2.1. General model

The general two-dimensional continuity, momentum and energy equations for the laminar thin film are given as

$$\frac{\partial u}{\partial x}+\frac{\partial v}{\partial y}=0 \tag{2}$$

$$\rho\left(\frac{\partial u}{\partial t}+u\frac{\partial u}{\partial x}+v\frac{\partial u}{\partial y}\right)=-\frac{\partial p}{\partial x}+\mu\left(\frac{\partial^2 u}{\partial x^2}+\frac{\partial^2 u}{\partial y^2}\right) \tag{3}$$

$$\rho\left(\frac{\partial v}{\partial t}+u\frac{\partial v}{\partial x}+v\frac{\partial v}{\partial y}\right)=-\frac{\partial p}{\partial y}+\mu\left(\frac{\partial^2 v}{\partial x^2}+\frac{\partial^2 v}{\partial y^2}\right) \tag{4}$$

$$\rho c_p\left(\frac{\partial T}{\partial t}+u\frac{\partial T}{\partial x}+v\frac{\partial T}{\partial y}\right)=k\left(\frac{\partial^2 T}{\partial x^2}+\frac{\partial^2 T}{\partial y^2}\right) \tag{5}$$

where T, ρ, p, μ, c_p and k are the fluid temperature, density, pressure, dynamic viscosity, specific heat and the thermal conductivity of the fluid, respectively.

A generalized set of boundary and initial conditions for this problem are

$$\begin{aligned}
&u(x,0,t)=0, \quad u(x,h,t)=0,\\
&v(x,0,t)=0, \quad v(x,h,t)=h_0\omega\gamma\beta\sin(\gamma\omega t)\\
&\frac{\partial p(0,y,t)}{\partial x}=C_1, \quad p(B,y,t)=p_e\\
&T(x,0,t)=T_2\\
&T(x,h,t)=T_2, \quad T(0,y,t)=T_1,\\
&\frac{\partial T(B,y,t)}{\partial x}=0, \quad T(x,y,0)=T_1
\end{aligned} \tag{6a}$$

where p_e, T_1 and T_2 are application specified constants. When the value of C_1 is set to zero, there will be no flow entering or leaving the thin film at $x=0$. However, negative values of C_1 insure that flow is always entering the thin film. The constant C_1 is function of time and will be determined later based on the assumption that the average velocity at the inlet is constant. This assumption can find its applications in thin films having flows driven by gravity such as in the fluidic cells used by Raiteri et al. [7].

Another set of thermal boundary and initial conditions corresponding to UHF that will be considered are

$$\begin{aligned}
&T(x,y,0)=T_1, \quad T(0,y,t)=T_1, \quad -k\frac{\partial T(x,0,t)}{\partial y}=q,\\
&\frac{\partial T(x,h,t)}{\partial n}=0 \quad \frac{\partial}{\partial x}\left(\frac{T_W(B,t)-T(B,y,t)}{T_W(B,t)-T_m(B,t)}\right)\cong 0
\end{aligned} \tag{6b}$$

where q, u_m and n are a constant represents the heat flux applied at the lower plate, the mean axial velocity at the exit and the direction normal to the upper plate, respectively. It is assumed that the upper plate is insulated which can model certain applications like biological fluidic cells that require isolation from the external environment. Note that T_W and T_m are the temperature of the lower plate and the mean bulk temperature which are defined later. The suggested exit thermal boundary condition as shown in condition (6b) was proven in the literature for steady state conditions (see Edwards et al. [8]). Also, it was shown numerically in the work of Khaled and Vafai [6] that this condition represents a good approximation for the exit thermal condition for flat sinusoidally squeezed thin films.

2.2. Low Reynolds numbers flow model

Eqs. (2)–(5) are non-dimensionalized using the following dimensionless variables:

$$X=\frac{x}{B}, \quad Y=\frac{y}{h_0} \tag{7a, b}$$

$$\tau=\omega t \tag{7c}$$

$$U=\frac{u}{(\omega B+V_0)}, \quad V=\frac{v}{h_0\omega} \tag{7d, e}$$

$$\Pi = \frac{p - p_e}{\mu\left(\omega + \frac{V_0}{B}\right)\varepsilon^{-2}} \tag{7f}$$

$$\theta = \frac{T - T_1}{\Delta T} \tag{7g}$$

where T_1 and V_0 are the temperature of the fluid at the inlet and a constant representing a reference dimensional inlet velocity, respectively. ΔT is equal to $T_2 - T_1$ for CWT conditions and it is equal to qh_0/k for UHF conditions. The variables X, Y, τ, U, V, Π and θ are the dimensionless forms of x, y, t, u, v, p and T variables, respectively. The above transformations except for dimensionless temperature have been used by Langlois [2] along with the following perturbation parameter:

$$\varepsilon = \frac{h_0}{B} \tag{8}$$

where h_0 is a reference thin film thickness.

The resulting first-order dimensionless continuity and momentum equations are

$$\frac{\partial U}{\partial X} + \frac{1}{\left(1 + \frac{V_0}{\omega B}\right)}\frac{\partial V}{\partial Y} = 0 \tag{9}$$

$$\frac{\partial \Pi}{\partial X} = \frac{\partial^2 U}{\partial Y^2} - R_S\frac{\partial U}{\partial \tau} - (R_S + R_L)\left[U\frac{\partial U}{\partial X}\right] - R_S V\frac{\partial U}{\partial Y} \tag{10}$$

$$\frac{\partial \Pi}{\partial Y} = 0 \tag{11}$$

where R_S and R_L are squeezing and lateral Reynolds numbers, respectively. They are given as

$$R_S = \frac{\rho h_0^2 \omega}{\mu}, \quad R_L = \frac{\rho V_0 h_0}{\mu}\left(\frac{h_0}{B}\right) \tag{12a, b}$$

The solution to Eq. (10) for low Reynolds numbers in absence of any boundary translational effects is

$$U = \frac{1}{2}\frac{\partial \Pi}{\partial X}(Y)(Y - H) \tag{13}$$

Eq. (13) along with Eq. (9) can be solved to determine the Reynolds equation [9]

$$\frac{\partial}{\partial X}\left(H^3\frac{\partial \Pi}{\partial X}\right) = \sigma\frac{\partial H}{\partial \tau} \tag{14}$$

where σ is the squeezing number and it is equal to

$$\sigma = \frac{12}{1 + \frac{V_0}{\omega B}} \tag{15}$$

Eq. (13) reduces to the following after solving Eq. (14):

$$U(X, Y, \tau) = \frac{1}{2H}[\sigma\beta\gamma X\sin(\gamma\tau) + C_1^*]\left(\frac{Y}{H}\right)\left(\frac{Y}{H} - 1\right) \tag{16a}$$

The corresponding normal velocity is found to be by solving Eq. (9)

$$V(X, Y, \tau) = \left[-2\left(1 - \frac{3\kappa X}{H}\right)\left(\frac{Y}{H}\right)^3 + 3\left(1 - \frac{2\kappa X}{H}\right)\left(\frac{Y}{H}\right)^2\right]\beta\gamma\sin(\gamma\tau) + \frac{6C_1^*\kappa}{\sigma H}\left[\left(\frac{Y}{H}\right)^3 - \left(\frac{Y}{H}\right)^2\right] \tag{17a}$$

The constant C_1^* can be obtained by equating the flow rate at the inlet calculated by integrating Eq. (16a) at $X = 0$ to the average velocity at the inlet which is assumed to be constant (i.e. reference axial velocity V_0) multiplied by the inlet film thickness. This results C_1^* to equal to $-(12 - \sigma)H(0, \tau)$. Accordingly, Eqs. (16a) and (17a) are can be written as

$$U(X, Y, \tau) = \frac{1}{2H}[\sigma\beta\gamma X\sin(\gamma\tau) - (12 - \sigma)H(0, \tau)]\left(\frac{Y}{H}\right)\left(\frac{Y}{H} - 1\right) \tag{16b}$$

$$V(X, Y, \tau) = \beta\gamma\sin(\gamma\tau)\left[3\left(1 - \frac{2\kappa X}{H}\right)\left(\frac{Y}{H}\right)^2 - 2\left(1 - \frac{3\kappa X}{H}\right)\left(\frac{Y}{H}\right)^3\right] - 6\left(\frac{12}{\sigma} - 1\right) \times \frac{\kappa H(0, \tau)}{H}\left[\left(\frac{Y}{H}\right)^3 - \left(\frac{Y}{H}\right)^2\right] \tag{17b}$$

Next, Eq. (5) is reduced to the following when dimensionless variables (7) and (8) are used

$$P_S\left(\frac{\partial \theta}{\partial \tau} + \frac{12}{\sigma}U\frac{\partial \theta}{\partial X} + V\frac{\partial \theta}{\partial Y}\right) = \varepsilon^2\frac{\partial^2 \theta}{\partial X^2} + \frac{\partial^2 \theta}{\partial Y^2} \tag{18}$$

where P_S is the thermal squeezing parameter and it is defined as follows:

$$P_S = R_S Pr \tag{19}$$

where $Pr = \rho c_p \upsilon/k$ is the Prandtl number of the fluid.

2.3. Large squeezing Reynolds number flow model

It is convenient to solve the vorticity equation and stream function formulations for cases with large squeezing Reynolds numbers. These equations are listed below in dimensional form:

$$\frac{\partial \Omega}{\partial t} + u\frac{\partial \Omega}{\partial x} + v\frac{\partial \Omega}{\partial y} = \upsilon\left(\frac{\partial^2 \Omega}{\partial x^2} + \frac{\partial^2 \Omega}{\partial y^2}\right) \tag{20}$$

$$\frac{\partial^2 \Psi}{\partial x^2} + \frac{\partial^2 \Psi}{\partial y^2} = -\Omega \tag{21}$$

where Ω and Ψ are the dimensional vorticity and stream functions, respectively. The vorticity and stream func-

tions are related to the velocity components through the following:

$$\Omega = \frac{\partial v}{\partial x} - \frac{\partial u}{\partial y} \tag{22}$$

$$u = \frac{\partial \Psi}{\partial y}, \quad v = -\frac{\partial \Psi}{\partial x} \tag{23a, b}$$

The following dimensionless variables are suggested

$$X = \frac{x}{B}, \quad Y = \frac{y}{h_0} \tag{24a, b}$$

$$\tau = \omega t \tag{24c}$$

$$\Omega^* = \frac{\Omega}{(V_0 + \omega B)/h_0}, \quad \Psi^* = \frac{\Psi}{h_0(V_0 + \omega B)} \tag{24d, e}$$

$$\theta = \frac{T - T_1}{\Delta T} \tag{24f}$$

where Ω^* and Ψ^* are the corresponding dimensionless values for Ω and Ψ, respectively. The introduction of variable (24e) in Eqs. (23a,b) results in the following dimensionless velocity components:

$$U = \frac{u}{V_0 + \omega B}, \quad V = \frac{v}{\varepsilon(V_0 + \omega B)} \tag{25a, b}$$

The dimensionless vorticity–stream function formulations for the flow inside the thin film and the dimensionless energy equation are

$$\left(\frac{\partial \Omega^*}{\partial \tau} + \left(1 + \frac{R_L}{R_S}\right)\left(\frac{\partial \Psi^*}{\partial Y}\frac{\partial \Omega^*}{\partial X} - \frac{\partial \Psi^*}{\partial X}\frac{\partial \Omega^*}{\partial Y}\right)\right) = \frac{1}{R_S}\left(\varepsilon^2 \frac{\partial^2 \Omega^*}{\partial X^2} + \frac{\partial^2 \Omega^*}{\partial Y^2}\right) \tag{26}$$

$$\left(\varepsilon^2 \frac{\partial^2 \Psi^*}{\partial X^2} + \frac{\partial^2 \Psi^*}{\partial Y^2}\right) = -\Omega^* \tag{27}$$

$$P_S\left(\frac{\partial \theta}{\partial \tau} + \left(1 + \frac{R_L}{R_S}\right)\left(\frac{\partial \Psi^*}{\partial Y}\frac{\partial \theta}{\partial X} - \frac{\partial \Psi^*}{\partial X}\frac{\partial \theta}{\partial Y}\right)\right) = \varepsilon^2 \frac{\partial^2 \theta}{\partial X^2} + \frac{\partial^2 \theta}{\partial Y^2} \tag{28}$$

The following transformations are used to avoid time and spatial dependent grid points:

$$\tau^* = \tau, \quad \xi = X \tag{29a, b}$$

$$\eta = \frac{Y}{H(X, \tau)} \tag{29c}$$

The boundary conditions can then be easily written in the dimensionless form in terms of the squeezing number as the following for the stream function formulation Eq. (27):

$$\Psi^*(0, \eta, \tau^*) = \left(1 - \frac{\sigma}{12}\right) H(0, \tau^*)\eta, \quad \frac{\partial^2 \Psi^*(1, \eta, \tau^*)}{\partial \xi^2} \cong 0 \tag{30a, b}$$

$$\Psi^*(\xi, 0, \tau^*) = 0 \tag{30c}$$

$$\Psi^*(\xi, 1, \tau^*) = \left(1 - \frac{\sigma}{12}\right) H(0, \tau^*) - \left(\frac{\sigma}{12}\right)\xi\beta\gamma \sin(\gamma\tau^*) \tag{30d}$$

while the next are the boundary conditions for the vorticity equation (26)

$$\Omega^*(0, \eta, \tau^*) = -\varepsilon^2\left(\frac{\partial^2 \Psi^*(0, \eta, \tau^*)}{\partial \xi^2} + \frac{2\eta\kappa^2}{H^2(0, \tau^*)}\frac{\partial \Psi^*(0, \eta, \tau^*)}{\partial \eta} - \frac{2\eta\kappa}{H(0, \tau^*)}\frac{\partial^2 \Psi^*(0, \eta, \tau^*)}{\partial \xi \partial \eta}\right) \tag{31a}$$

$$\frac{\partial \Omega^*(1, \eta, \tau^*)}{\partial \xi} \cong \left[\frac{C_4(1 - \beta\cos(\gamma\tau^*) - \kappa) - 2C_3\kappa}{(C_3 + C_4)(1 - \beta\cos(\gamma\tau^*) + \kappa)}\right]\Omega^*(1, \eta, \tau^*) \tag{31b}$$

$$\Omega^*(\xi, 0, \tau^*) = -\frac{\partial U(\xi, 0, \tau^*)}{H\partial \eta}, \quad \Omega^*(\xi, 1, \tau^*) = -\frac{\partial U(\xi, 1, \tau^*)}{H\partial \eta} \tag{31c, d}$$

Boundary conditions (30b) and (31b) are approximated boundary conditions derived based on the fact that the upper plate is slightly inclined and that the velocity at the exit of the thin film has the following order of magnitude:

$$U \approx \frac{C_3 + C_4\xi}{H} p(\eta) \tag{32}$$

where $p(\eta)$ is a certain function of η. The parameters C_3 and C_4 are

$$C_3 = \left(1 - \frac{\sigma}{12}\right) H(0, \tau^*), \quad C_4 = -\left(\frac{\sigma}{12}\right)\beta\gamma \sin(\gamma\tau^*) \tag{33a, b}$$

The thermal boundary conditions for plates having a CWT are

$$\theta(\xi, 0, \tau^*) = 1, \quad \theta(\xi, 1, \tau^*) = 1 \tag{34a, b}$$

$$\theta(0, \eta, \tau^*) = 0, \quad \frac{\partial \theta(1, \eta, \tau^*)}{\partial \xi} = \frac{\kappa\eta}{H}\frac{\partial \theta(1, \eta, \tau^*)}{\partial \eta} \tag{34c, d}$$

while the corresponding thermal boundary conditions for uniform heat flux conditions at the thin film plates are

$$\frac{\partial \theta(\xi, 0, \tau^*)}{H\partial \eta} = -1, \quad \frac{\partial \theta(\xi, 1, \tau^*)}{\partial \eta} = \frac{\varepsilon^2\kappa H}{1 + \varepsilon^2\kappa^2}\frac{\partial \theta(\xi, 1, \tau^*)}{\partial \xi} \tag{35a, b}$$

$$\theta(0, \eta, \tau^*) = 0 \tag{35c}$$

$$\frac{\partial\theta(1,\eta,\tau^*)}{\partial\xi} = \frac{\kappa\eta}{H}\frac{\partial\theta(1,\eta,\tau^*)}{\partial\eta} + \frac{\partial\theta_W(1,\tau^*)}{\partial\xi} - \left[\frac{\theta_W(1,\tau^*)-\theta(1,\eta,\tau^*)}{\theta_W(1,\tau^*)-\theta_m(1,\tau^*)}\right] \times \left[\frac{\partial\theta_W(1,\tau^*)}{\partial\xi} - \frac{\partial\theta_m(1,\tau^*)}{\partial\xi}\right] \quad (35d)$$

where θ_m and θ_W are the dimensionless mean bulk and lower plate's temperatures, respectively. Eq. (35d) can be used for CWT conditions for relatively large P_S values noting that $\theta_W(1,\tau^*)=1$ in this case. The boundary conditions (35b) is obtained by resolving the temperature gradient at the upper plate along the η-direction since the upper plate is insulated.

2.4. Calculated parameters

The calculated thermal parameters that will be considered are the Nusselt numbers at the lower and upper plates. They are defined according to the following equations:

CWT

$$Nu_U(X,\tau) \equiv \frac{h_{cU}h_0}{k} = \frac{1}{1-\theta_m(X,\tau)}\left(\left(\frac{\partial\theta(X,H,\tau)}{\partial Y}\right)^2 + \varepsilon^2\left(\frac{\partial\theta(X,H,\tau)}{\partial X}\right)^2\right)^{1/2}$$
$$Nu_L(X,\tau) \equiv \frac{h_{cL}h_0}{k} = \frac{-1}{1-\theta_m(X,\tau)}\frac{\partial\theta(X,0,\tau)}{\partial Y} \quad (36)$$

UHF

$$Nu_L(X,\tau) \equiv \frac{h_{cL}h_0}{k} = \frac{1}{\theta(X,0,\tau)-\theta_m(X,\tau)} \quad (37)$$

$$\theta_m(X,\tau) = \frac{1}{U_m(X,\tau)H}\int_0^H U(X,Y,\tau)\theta(X,Y,\tau)\,dY$$
$$U_m(X,\tau) = \frac{1}{H}\int_0^H U(X,Y,\tau)\,dY \quad (38)$$

where U_m is the average dimensionless axial velocity. h_{cU} and h_{cL} are the convective heat transfer coefficient at the upper and the lower plates, respectively.

3. Numerical analysis

Eqs. (18), (26) and (28) are first transformed to the new computational domain (ξ,η,τ^*) and then solved using the alternating direction implicit method (ADI), see Ref. [10]. After each half time step for Eqs. (26) and (28), Eq. (27) was solved using the method of successive over relaxation SOR. The dimensionless velocities in Eq. (26) as well as the dimensionless vorticity at the plates of the thin film, seen in Eqs. (31c,d), were calculated initially at previous half time steps and then corrected by consecutive iterations until the convergence criteria is satisfied.

In the numerical results, the value of the dimensionless frequency was chosen to be 3.0. Note that other values will result in similar physical behavior. Based on extensive numerical experimentation for the large Reynolds number model, the values of 0.0125, 0.05, 0.001 and 10^{-5} were chosen for $\Delta\xi$, $\Delta\eta$, $\Delta\tau^*$ and the maximum error for stream functions in Eq. (27), respectively. However, a finer mesh was selected for the low Reynolds number model because less computational time is needed for this model. For highly convective cases, thermal and momentum axial diffusions can be neglected compared to axial convections and therefore errors associated with exit boundary conditions was found to be negligible.

The time history of the exit Nusselt number for both models was compared for similar controlling parameters for UHF conditions except for R_S which is allowed to vary from a negligible value to a value of 10 keeping a constant value for the thermal squeezing parameter. Both models were found to give a good agreement as shown in Fig. 2. The difference between the results is ascribed to additional inertia effects that are present in the high Reynolds number flow model. Also, different mesh sizes were used for both models. Accordingly, a parametric study is performed to investigate flow and heat transfer inside non-flat thin films.

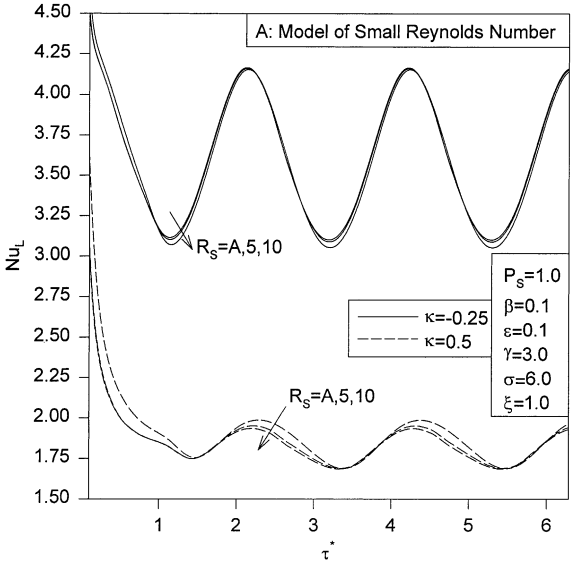

Fig. 2. Comparison between small and large Reynolds models (UHF).

4. Discussions of the results

4.1. Low Reynolds numbers flow model

Figs. 3 and 4 illustrate the effect of dimensionless slope of the upper plate of the thin film κ on the Nusselt number for CWT and UHF conditions, respectively. It is noticed that all Nu_L and Nu_U for CWT condition and Nu_L for UHF condition have oscillatory behaviors. Note that Nu_U is zero for the UHF condition. Further, both Nu_L and Nu_U for CWT condition and Nu_L for UHF condition decrease as κ increases due to a decrease in the average axial velocity as κ increases. An interesting feature for inclined thin films is that the variation in the Nusselt number decreases as κ increases. This can be recognized from Figs. 3 and 4. Moreover, it is noticed from Fig. 3 that Nu_U is always greater than Nu_L for convergent thin films while the opposite is true for divergent thin films.

As initial thermal effects diminish, kinks are noticed to appear for Nusselt numbers as in Figs. 2 and 3 due to the transition with the steady periodic solution. These are clear for divergent thin films and at larger σ values. This is because the increased fluid volume in divergent cells and the decreased inlet velocities for larger σ values increases the transient effects and accordingly we see these kinks occur at further times. These kinks can be seen in many vibrated dynamical systems.

The axial distribution of Nu_L at two different times is shown in Figs. 5 and 6 for CWT and UHF conditions, respectively. Nu_L is almost constant for $\kappa = 0.0$ except near the inlet where the flow is not thermally developed. However for cases where κ is different than zero, Nu_L increases almost linearly as ξ increases far from the inlet for negative values of κ and it decreases almost linearly for positive values of κ as ξ increases. The influence of κ on θ_m is shown in Fig. 7 for CWT condition. The values of θ_m are noticed to increase as κ decreases due to increases in the convective heat transfer coefficient. It can be seen for UHF conditions (Fig. 8) that average lower plate temperature θ_W is found to increase as κ increases due to a decrease in the convective heat transfer coefficient. Further, it is noticed that the average θ_W has an

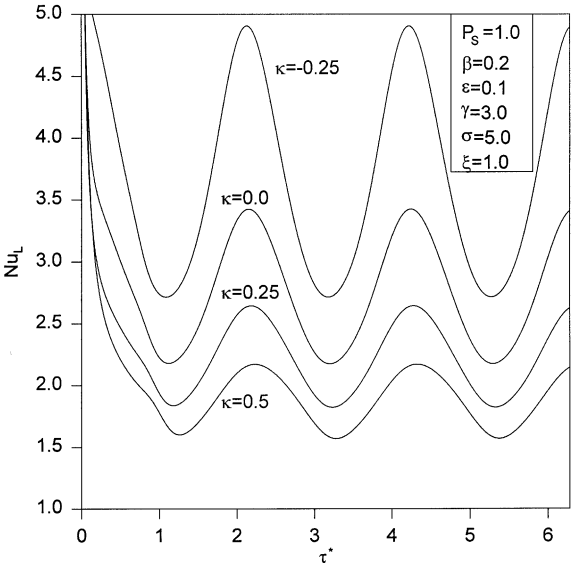

Fig. 4. Effects of κ on Nu (UHF).

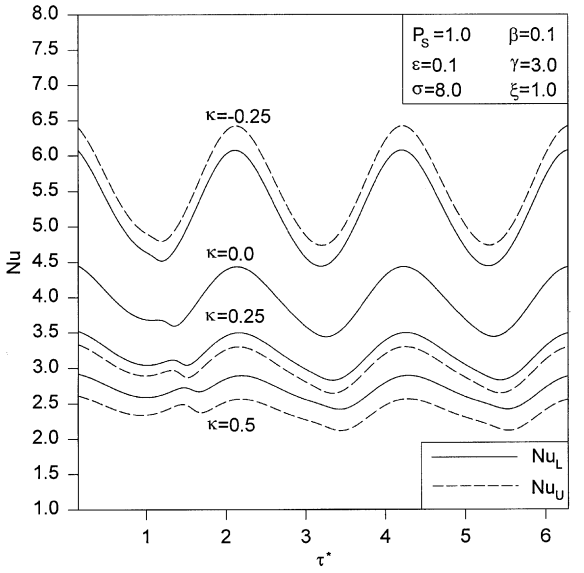

Fig. 3. Effects of κ on Nu (CWT).

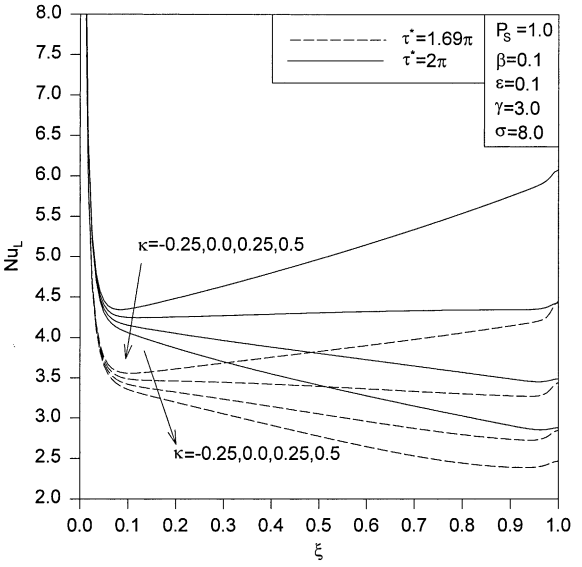

Fig. 5. Effects of κ on the development of Nu_L (CWT).

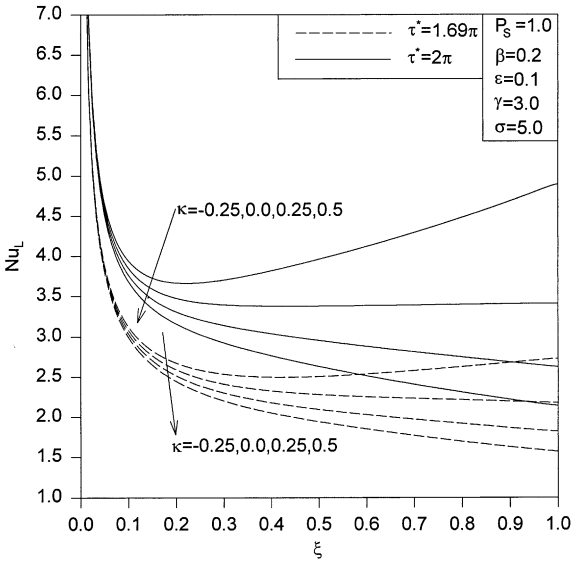

Fig. 6. Effects of κ on the development of Nu_L (UHF).

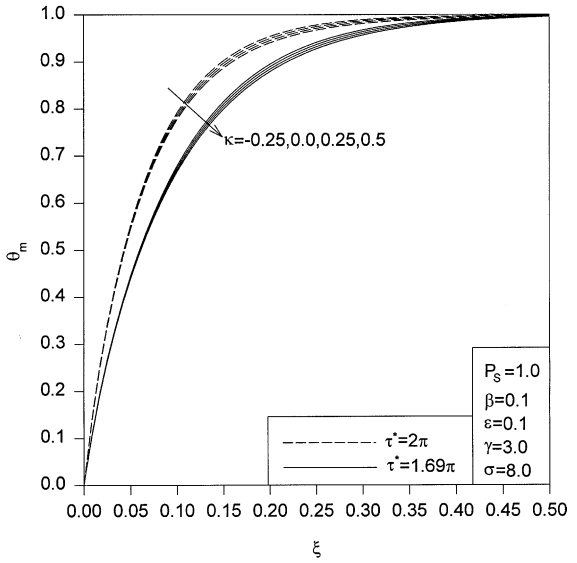

Fig. 7. Effects of κ on θ_m (CWT).

oscillatory behavior almost similar to the upper plate motion with a phase shift.

4.2. Correlations

The mean value of the Nusselt number Nu_m and the fluctuation in the Nusselt number are defined as follows:

$$Nu_m(X) = \frac{\gamma}{2\pi}\int_{2\pi(1-(1/\gamma))}^{2\pi} Nu(X,\tau^*)\,d\tau^* \tag{39}$$

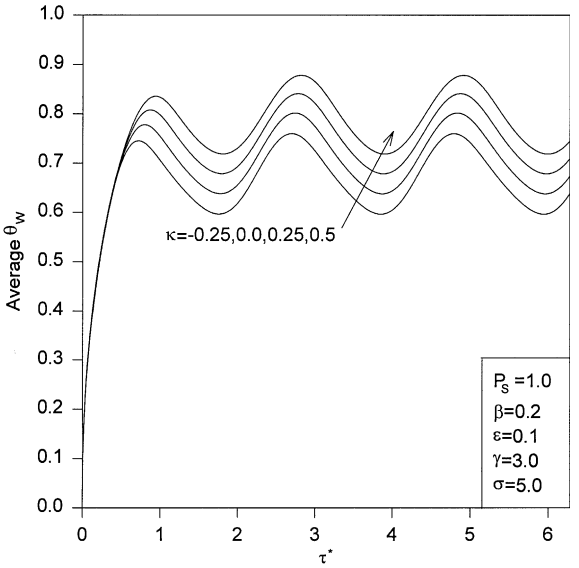

Fig. 8. Effects of κ on average θ_W (UHF).

$$\Delta Nu = \frac{(Nu_{max} - Nu_{min})}{2} \tag{40}$$

Table 1 contains correlations for both the mean value of the Nusselt number and its corresponding fluctuation. The maximum error between these correlations and the numerical results are 3% for the Nusselt numbers and about 6% for the values of $\Delta Nu_L/Nu_{L_m}$ and $\Delta Nu_U/Nu_{U_m}$.

The following equation characterizes of the Nusselt number variations for both CWT and UHF conditions

Table 1
Correlations for the mean Nusselt numbers and fluctuations in Nusselt numbers: ($P_S = 1.0$, $\epsilon = 0.1$ and $\sigma = 5.0$; $0.1 \leqslant \beta \leqslant 0.4$, $-0.25 \leqslant \kappa \leqslant 0.5$)

Condition	Correlations
CWT	$Nu_{L_m} = 3.853e^{-0.004\kappa X}[(1+\kappa X)^2 - \beta^2]^{-0.497}$
	$\frac{\Delta Nu_L}{Nu_{L_m}} = 1.674e^{-0.678\kappa X}(0.0478+\beta)^{1.361}$
CWT	$Nu_{U_m} = 3.846e^{-0.194\kappa X}[(1+\kappa X)^2 - \beta^2]^{-0.496}$
	$\frac{\Delta Nu_U}{Nu_{U_m}} = 1.675e^{-0.610\kappa X}(0.0468+\beta)^{1.356}$
UHF	$Nu_{L_m} = 2.719e^{0.117\kappa X}[(1+\kappa X)^2 - \beta^2]^{-0.519}$
	$\frac{\Delta Nu_L}{Nu_{L_m}} = 1.187e^{-1.163\kappa X}\beta^{1.026}$

as a function of dimensionless time τ^* in the absence of transient effects and viscous dissipation.

$$Nu_L(X,\tau) = \frac{Nu_{L_m}(X,\tau)\sqrt{(1+\kappa X)^2-\beta^2}}{(1-\beta\cos(\gamma\tau)+\kappa X)} \quad (41)$$

The values of Nu_{L_m} in Eq. (41) are obtained from Table 1 and can be used for different σ and P_S values as long as the Nusselt number is evaluated far from the inlet. In this region, the flow can be said to be thermally fully developed. Eq. (41) can also be applied for evaluating the Nusselt number at the upper plate for CWT conditions.

4.3. Large squeezing Reynolds number flow model

Fig. 9 shows the effects of R_S on the dimensionless velocity profiles at maximum relief velocity for a flat thin film. Although the average velocity for the studied case is positive, negative velocities appear near the lower plate for R_S greater than 40 as shown in Fig. 9. This instability or flow separation is due to reductions in the flow kinetic energy and increases in fluid pressure as a result of upper plate relaxation. The critical R_S value that causes flow separations near the plates decreases as the dimensionless slope κ increases as shown in Fig. 10.

Figs. 11 and 12 explain the influences of dimensionless slope of the upper plate κ on the axial and normal velocity profiles at the exit of the thin film, respectively. Axial velocities and the corresponding shear rates increase as κ decreases as illustrated in Fig. 11. For undisturbed thin films, the minimum normal velocities are

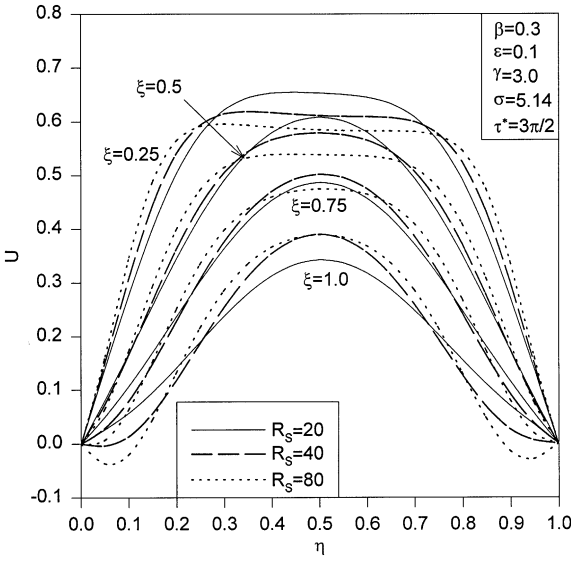

Fig. 9. Effects of R_S on U profiles (high R_S).

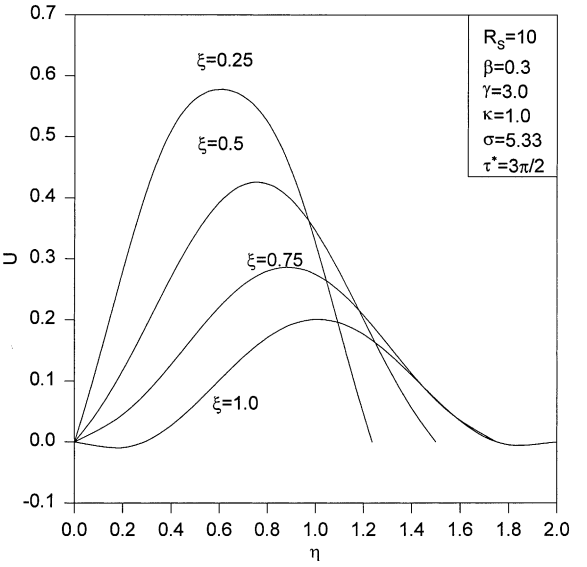

Fig. 10. U profiles for large κ value.

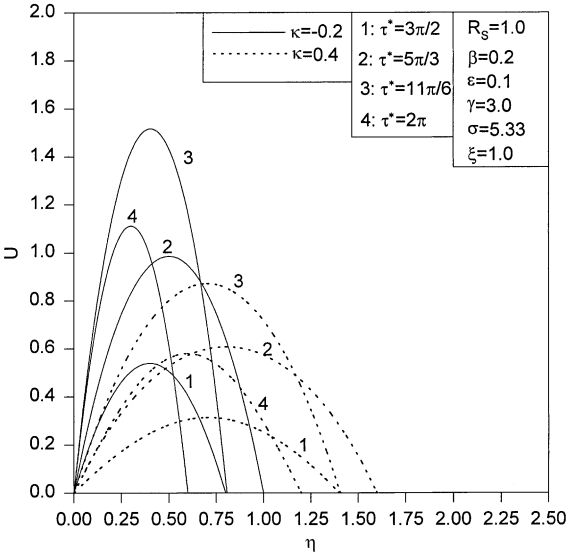

Fig. 11. Effects of κ on U.

for flat thin films but convergent thin films have higher normal velocities than divergent ones because these velocities are proportional to the gradient of the axial velocities which is proportional to $\kappa/(\kappa+1)^2$. Yet the variation in normal velocities near the fixed plate of squeezed thin films can be minimized significantly for divergent thin films. This can be seen from Fig. 12. Also, Eq. (17b) suggests that divergent cells having κ near unity have a minimized normal velocities near the lower plate for small values of β and at large values of σ.

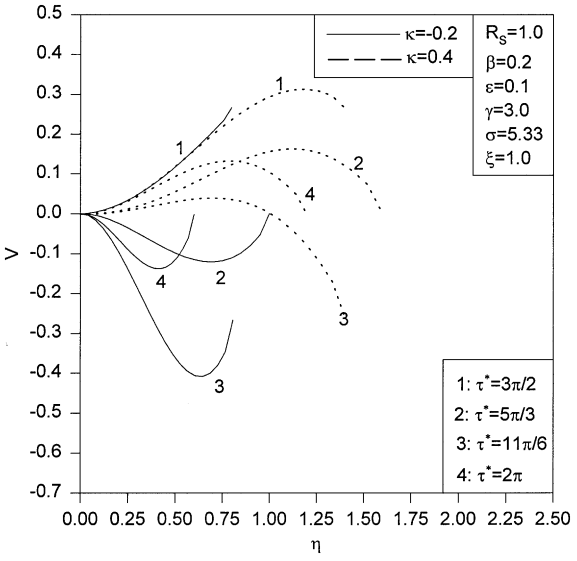

Fig. 12. Effects of κ on V.

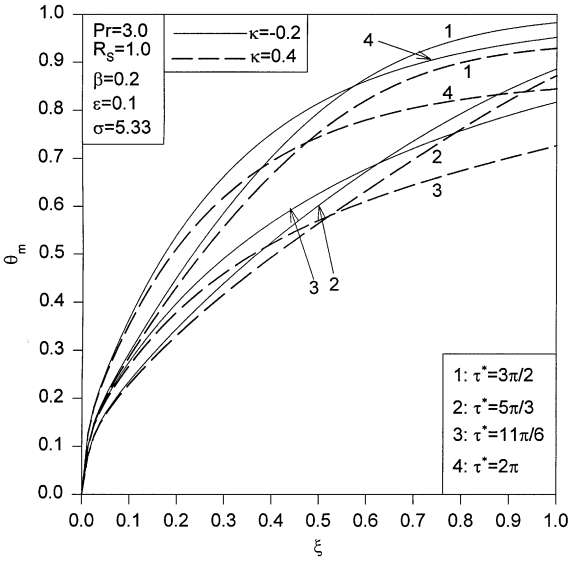

Fig. 13. Effects of κ on θ_m (large Pr, CWT).

The effects of κ on θ_m at dimensionless times $\tau^* = 3\pi/2$, $5\pi/3$, $11\pi/6$ and 2π is exemplified in Fig. 13 for CWT conditions. Values of θ_m for the studied convergent thin film, $\kappa = -0.2$, is found to be greater than those for the studied divergent thin film, $\kappa = 0.4$. The increased axial velocities in convergent thin films results in an increase in the convective heat transfer coefficient. This in turn increases the heat transfer to the fluid for CWT conditions. Accordingly, θ_m increases as κ decreases. It is further noticed from this figure that fluctuations in θ_m at the exit of the thin film increase as κ increases as in divergent thin films.

5. Conclusions

The effects of external squeezing of the upper plate of a thin film that has a linearly varying thickness with the horizontal distance have been considered on flow and heat transfer for a wide range of squeezing Reynolds numbers. In the present study, the governing equations have been non-dimensionalized and reduced to two categories: low and large Reynolds number flow models. Both categories were compared at a limiting case and were found to be in excellent agreement. It was found that flow instabilities and flow separation occur at lower squeezing Reynolds number for divergent thin films in contrast to convergent thin films. However, fluctuations in the axial and normal velocities were found to be greater for convergent thin films as compared to divergent thin films. Further, Nusselt numbers and their amplitudes were found to decrease when the dimensionless slope of the upper plate was increased. Convergent thin films were found to be thermally more stable as lubricating thin films, microchannels or fluidic cells of chemical or biological nanosensors. Finally the instability in the dynamic behavior of divergent thin films at large squeezing Reynolds numbers can for example eliminated by using magnetic devices at the exit.

References

[1] N.V. Lavrik, C.A. Tipple, M.J. Sepaniak, D. Datskos, Gold nano-structure for transduction of biomolecular interactions into micrometer scale movements, Biomed. Microdev. 3 (1) (2001) 35–44.

[2] W.E. Langlois, Isothermal squeeze films, Quart. Appl. Math XX (1962) 131–150.

[3] E.A. Hamza, Unsteady flow between two disks with heat transfer in the presence of a magnetic field, J. Phys. D: Appl. Phys. 25 (1992) 1425–1431.

[4] S. Bhattacharyya, A. Pal, G. Nath, Unsteady flow and heat transfer between rotating coaxial disks, Numer. Heat Transfer, Part A 30 (1996) 519–532.

[5] A.-R.A. Khaled, K. Vafai, Non-isothermal characterization of thin film oscillating bearings, Numer. Heat Transfer, Part A 41 (2002) 451–468.

[6] A.-R.A. Khaled, K. Vafai, Heat transfer and hydromagnetic control of flow exit conditions inside oscillatory squeezed thin films, Numer. Heat Transfer, Part A, in press.

[7] R. Raiteri, H.-J. Butt, M. Grattarola, Changes in surface stress at the liquid/solid interface measured with a microcantilever, Electrochim. Acta 46 (2000) 157–163.

[8] D.K. Edwards, V.E. Denny, A.F. Mills, Transfer Processes: An Introduction to Diffusion, Convection, and Radiation, Hemisphere, New York, 1979.
[9] O. Reynolds, On the theory of lubrication and its application to Mr. Beauchamp Tower's experiments, including an experimental determination of the viscosity of olive oil, Philos. Trans. R. Soc. Lond. 177 (1886) 157–237.
[10] K.A. Hoffmann, S.T. Chiang, Computational Fluid Dynamics: vol 1, third edition, Wichita, Kansas, Engineering Education System (1998) 337–352.